Crystal field analysis of Nd^{3+} energy levels in monoclinic $NdAl_3(BO_3)_4$ laser

2001 J. Phys.: Condens. Matter 13 8071

(http://iopscience.iop.org/0953-8984/13/35/314)

INSTITUTE OF PHYSICS PUBLISHING JOURNAL OF PHYSICS: CONDENSED MATTER

J. Phys.: Condens. Matter **13** (2001) 8071–8085 PII: S0953-8984(01)26128-1

Crystal field analysis of Nd^{3+} energy levels in monoclinic $NdAl_3(BO_3)_4$ laser

C Cascales[1], C Zaldo[1], U Caldiño[2], J García Solé[3] and Z D Luo[4]

[1] Instituto de Ciencia de Materiales de Madrid, Consejo Superior de Investigaciones Científicas, Cantoblanco, 28049 Madrid, Spain
[2] Departamento de Física, Universidad Autónoma Metropolitana, Iztapalapa, PO Box 55-534, 09340 México DF, Mexico
[3] Departamento de Física de Materiales, Universidad Autónoma de Madrid, Cantoblanco, 28049 Madrid, Spain
[4] Fujian Institute of Research on the Structure of Matter, Chinese Academy of Sciences, Fuzhou, Fujian 350002, People's Republic of China

Received 25 June 2001, in final form 18 July 2001
Published 16 August 2001
Online at stacks.iop.org/JPhysCM/13/8071

Abstract

The energies of 135 Kramers doublets extending up to the $^2H1_{11/2}$ multiplet for Nd^{3+} in a monoclinic $C2/c$ space group (No 15) $NdAl_3(BO_3)_4$ (NAB) single crystal laser have been determined from polarized optical absorption and photoluminescence measurements at 7 K. The strongly polarized character of the Nd spectra has been discussed under the assumption of a local D_3 symmetry, higher than the C_2 symmetry of NAB, and the observed energy levels have been labelled with the adequate crystal quantum numbers and irreducible representations. A detailed Hamiltonian of 21 parameters has been used in the simulation of the energy levels and associated wavefunctions of the $4f^3$ configuration of Nd^{3+}. The diagonalized complete energy matrix combines simultaneously the free-ion and single-particle crystal field interactions. Starting B_q^k CF parameters were calculated from the semi-empirical simple overlap model SOM. A comparative simulation considering the C_2 symmetry of NAB is provided. Moreover, two-electron CF interactions as well as an empirical correction have been tested in calculating the anomalous splitting of the $^2H2_{11/2}$ levels. A final fit in D_3 symmetry produces a very good adjustment with a low rms deviation $\sigma = 15.3$ cm^{-1} between observed and calculated energy levels.

1. Introduction

Neodymium aluminum borate $NdAl_3(BO_3)_4$, hereafter NAB, single crystal is a stoichiometric laser with weak quenching of the neodymium photoluminescence [1–3]. The high Nd^{3+}

concentration in the crystal ([Nd] $= 5.43 \times 10^{21}$ cm^{-3}) allows high optical absorption coefficients and therefore a reduction of the active crystal dimension below 0.1 mm.

The room temperature phase of NAB crystal can be selected by accurate control of the crystal growth temperature ([2], [4] and references therein). NAB has been reported to be isostructural with the mineral huntite, with the hexagonal symmetry of the S.G. *R*32 (No 155) [5], $Z = 3$, and unit-cell parameters (Å) $a = 9.3416(6)$, $c = 7.3055(8)$ and $V = 552.1$ Å^3, when grown up to 1289 ± 5 K. Nd^{3+} cations placed at 3a positions are surrounded by six O^{2-} ions of the same type, at 2.371 Å, forming distorted NdO_6 trigonal prisms with crystallographic symmetry D_3. Below this temperature, the phase of crystals grown up to 1195 ± 5 K has been described in the monoclinic S.G. $C2/c$ (No 15) [4, 6], with room temperature cell parameters (Å) $a = 7.262(3)$, $b = 9.365(3)$, $c = 11.138(7)$, $\beta = 103.41(4)^\circ$ and $V = 736.8(1)$ Å^3. In this case, Nd^{3+} in 4e positions is coordinated to six O^{2-} ions of three different types, at distances of about 2.40 Å, and its crystal environment is a distorted octahedron with crystallographic symmetry C_2. Finally, the existence of another phase, α-NAB, grown below 1195 K has been also reported [7, 8] with the monoclinic symmetry of the S.G. *C*2 (No 5).

To date, reported studies on optical properties of stoichiometric $RAl_3(BO_3)_4$, RAB, or R-doped $YAl_3(BO_3)_4$, YAB, R = trivalent lanthanide, seem to concern only the above described hexagonal form. In these crystals, some unexpected features of the optical spectra, i.e. the claimed presence of additional spectroscopic sites for R $= Er^{3+}$ and Dy^{3+} in RAB [9] have been attributed to the partial substitution in the Al and/or interstitial sites. The interpretation of satellite peaks appearing in the UV spectrum of $EuAl_3(BO_3)_4$ as originating from a possible C_2 symmetry site for Eu^{3+} in this borate host [10], was subsequently discarded from results of the spectroscopic study on Eu^{3+} in the YAB host [11].

Whereas optical spectra of Nd^{3+} in a hexagonal YAB host have been investigated at liquid-He temperature [12], studies for isostructural NAB are only available from measurements at temperatures equal to or above 77 K. In the latter case, the information provided is limited to the $^4I_{9/2}$, $^4I_{11/2}$ and $^4F_{3/2}$ energy levels inferred from photoluminescence [1]. Moreover, the previously suggested [1] small energy gap, 19 cm^{-1}, between the fundamental and first excited level of the ground $^4I_{9/2}$ multiplet, makes likely the observation of transitions from thermally populated excited levels at 77 K and therefore the assignment of experimental results to Nd^{3+} levels is ambiguous. Finally, the polarization character of the optical transitions is not known. In consequence, the interpretation of the presently available spectroscopic data for NAB is rather uncertain.

In this work the crystal-field CF analysis provides precise information on the Nd^{3+} energy levels and their corresponding wavefunctions in NAB as well as on the character of the transitions between these levels. The comparison between experimental and calculated results is used to confirm level assignments. This approach was also previously used in a detailed CF study for Eu^{3+} in YAB [11]. In contrast, previous attempts to parametrize the CF effects through *only* 13 energy levels from $^4I_{9/2}$, $^4I_{11/2}$ and $^4F_{3/2}$ multiplets in stoichiometric NAB [13], or 20 levels, when $^4I_{13/2}$ is also included, for doped Nd^{3+} YAB [13–15] have only a limited value.

The $4f^3$ configuration of Nd^{3+} is one of the most interesting from a spectroscopic approach since it offers both the maximum number of interactions to be studied and still a rather simple and conveniently calculable set of energy levels with only 182 Kramers levels. Given that the satisfactory reproduction of the configuration requires the use of a sufficiently detailed Hamiltonian including free-ion and CF interactions as well as the diagonalization of the *complete* energy matrix, the precise determination of the most extensive possible energy level sequence of Nd^{3+} would be required. Since the borate NAB host is transparent up to about 285 nm, the determination of a large number of experimental levels to perform the CF analysis is feasible.

The 135 Stark energy levels observed at 7 K for Nd^{3+} in NAB have been first labelled with the appropriate crystal quantum numbers m and irreducible representations (IRs) of an odd electron system with local D_3 point symmetry, and compared with the calculated ones obtained through a phenomenological single-particle model using an extensive Hamiltonian of 21 parameters, which includes simultaneously free-ion and CF interactions. The CF interactions are characterized through only six real B_q^k parameters. Subsequently the same kind of simulation was carried out in the real C_2 point site symmetry of Nd^{3+} in monoclinic NAB, for which nine real B_q^k and five complex S_q^k CF parameters must be considered. In this case, neither selection rules for optical transitions nor differentiated IR to the observed levels should be applied. Two-electron CF interactions as well as an empirical correction have been tested in calculating the anomalous splitting of the $^2H2_{11/2}$ state, for both considered symmetries. An evaluation of the consistency and physical meaning of D_3 and C_2 final sets of CF parameters can be envisaged from the comparison with both the collection reported for Eu^{3+} in YAB [11] and that obtained from semi-empirical SOM calculations considering crystal data. These phenomenological parametrizations of CF effects allow the unambiguous assignment of CF levels as well as discussion about the site symmetry and the possibility of additional sites.

2. Crystal properties and experimental details

Deep purple NAB single crystals have been grown by the flux method. Details of the crystal growth procedures can be found in a previous work [2]. The x-ray diffraction analysis was carried out on a Siemens SMART-CCD diffractometer using Mo Kα radiation. This confirms that our crystal corresponds to the monoclinic NAB phase, $C2/c$ (No 15) space group, and it provides the unit cell parameters $a = 7.253(2)$ Å, $b = 9.363(3)$ Å, $c = 11.121(3)$ Å, $\beta = 103.47(3)^\circ$ and $V = 734.4(4)$ Å^3, very close to those previously reported [4, 6]. The C_2 symmetry axis of the Nd^{3+} crystal position, the reference c-axis of the crystal-field potential, is parallel to the $\boldsymbol{b}$ direction of the lattice. Furthermore, the polyhedron surrounding Nd^{3+} is not far from a trigonal prism, since Nd^{3+} is in 4e $(x, y, 1/4)$ sites, with y very near 0, and the three Nd^{3+}–O distances from its three kinds of linked oxygen in 8f (x, y, z) sites have (nearly) the same values, thus a local pseudo-D_3 symmetry around Nd^{3+} can be also envisaged. Figure 1 sketches the comparison of the oxygen polyhedra around Nd in both symmetries. According to the conventions of Prather [16] the simplest way to describe a CF potential is to choose a reference axis system for which the c-axis corresponds to the highest possible symmetry axis. In the case of D_3 symmetry this c-axis is a local threefold axis, perpendicular to the C_2 crystallographic axis in the unit cell. From the above point of view, σ ($E \perp c$; $B \parallel c$) and π ($E \parallel c$; $B \perp c$) polarized optical absorption and photoluminescence spectra were recorded using a thin plate of NAB cut with the c-axis contained in its main faces.

The $^{2S+1}L_J$ multiplets of Nd^{3+} in NAB with energy equal to or above $^4I_{13/2}$ have been determined from 7 K optical absorption measurements performed in a Varian 5E spectrophotometer using a liquid helium flux Oxford cryostat model SU12. The energy of sublevels not accessible by optical absorption in our spectrophotometer, i.e. $^4I_{9/2}$ and $^4I_{11/2}$, have been deduced from 10 K emission of the $^4F_{3/2}$. In that case, the photoluminescence was excited with a Ti-sapphire laser, the emission dispersed with a 500 M Spex monochromator and the signal recorded with suitable detectors, a Hamamatsu R636 photomultiplier ($^4I_{9/2}$) and cooled Ge photodiode ($^4I_{11/2}$), using the lock-in amplifying technique.

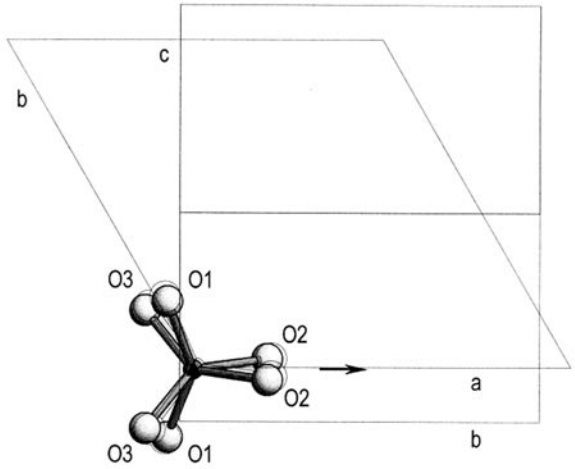

Figure 1. Comparison of coordination polyhedra of Nd^{3+} in the R32 hexagonal structure, as seen in the *ab* plane along the *c* direction, and in monoclinic $C2/c$, in the *bc* plane along the *a* direction. Shadowed circles correspond to O1, O2 and O3 ions of the monoclinic phase, while transparent circles correspond to the equivalent oxygens in the hexagonal structure. Nd is kept at the same position in both structures. The arrow indicates the C_2 axis and the triangle on Nd indicates the C_3 axis.

3. Parametric energy level analysis

The effect of the different interactions responsible for the energy levels structure, intraionic H_{FI} as well as CF effects arising from the influence of the surrounding charges on the $4f^3$ electrons, can be described with a combined Hamiltonian $H_T = H_{FI} + H_{CF}$ which includes one or several parameters for each interaction [17]

$$H_T = H_0 + \sum_{k=0,1,2,3} E^k e_k + \zeta_{4f} A_{SO} + \alpha L(L+1) + \beta G(G_2) + \gamma G(R_7) + \sum_{k=0,2,4} M^k m_k + \sum_{i=2,4,6} P^i p_i + \sum_{\lambda=2,3,4,6,7,8} T^\lambda t_\lambda + \sum_{k,q,i} B_q^k C_q^k(i).$$

In the H_{FI} free-ion part of this expression H_0 stands for the spherically symmetric one-electron term of the Hamiltonian. The Racah parameters E^k and the spin–orbit coupling interaction $\zeta_{4f} A_{SO}$ describe the electrostatic repulsion between equivalent f electrons and the coupling which results from the interaction between the spin magnetic moment of the electron and the magnetic field created by the movement of the electron around the nucleus, respectively. ζ_{4f} is the spin-orbit coupling constant. The so called Trees parameters α, β and γ, and Judd parameters T^λ, are accounting for the two- and three-body terms for the configuration interactions, respectively. Magnetically correlated corrections such as spin–spin and spin–other-orbit interactions can be simulated through the M^k parameters, also called Marvin integrals. Finally, the electrostatically correlated spin-orbit interactions are described by the P^i integrals.

In the one-electron CF part of the total Hamiltonian, C_q^k are related to the spherical tensors of rank k, dependent on the coordinates of the ith electron with summation over the three 4f electrons, and B_q^k are the CF parameters, whose k and q values are constrained by the symmetry of the centre site. Considering the local D_3 symmetry of Nd^{3+} in monoclinic NAB the potential

of the CF is

$$H_{D_3}(\text{even}) = B_0^2C_0^2 + B_0^4C_0^4 + B_3^4(C_{-3}^4 - C_3^4) + B_0^6C_0^6 + B_3^6(C_{-3}^6 - C_3^6) + B_6^6(C_{-6}^6 + C_6^6).$$

We can also express the same CF potential with reference to the C_2 axis, orthogonal to the threefold one. The Hamiltonian is now written as

$$\begin{aligned} H_{C_2}(\text{even}) = {} & B_0^2C_0^2 + B_2^2(C_{-2}^2 + C_2^2) + S_2^2(C_{-2}^2 - C_2^2) + B_0^4C_0^4 + B_2^4(C_{-2}^4 + C_2^4) \\ & + S_2^4(C_{-2}^4 - C_2^4) + B_4^4(C_{-4}^4 + C_2^4) + S_4^4(C_{-4}^4 - C_2^4) + B_0^6C_0^6 \\ & + B_2^6(C_{-2}^6 + C_2^6) + S_2^6(C_{-2}^6 - C_2^6) + B_4^6(C_{-4}^6 + C_4^6) + S_4^6(C_{-4}^6 - C_4^6) \\ & + B_6^6(C_{-6}^6 + C_6^6) + S_6^6(C_{-6}^6 - C_6^6). \end{aligned}$$

In the first case, only six real B_q^k CF parameters are nonzero, whereas for the C_2 potential nine real and five (S_2^2 is set to zero) complex S_q^k CF parameters must be considered. In order to find the relation between these two parameter sets, we consider that under a rotation of the reference axis system, the 'new' spherical harmonics should be written as a linear combination of the 'old' ones of the same rank. For this study we constructed the transformation matrix $D_3 \rightarrow C_2$, table 1, by using the quantitative expression of tensorial operators as given by Prather [16]. In this way, our fitting method will consist in the well known descending symmetry procedure. However, we must keep in mind that since recorded spectra reflect strongly polarized characteristics for the optical center, which will be described in the next paragraph, the current situation is just the opposite to the usual [18–20], i.e. Nd^{3+} in our monoclinic NAB is really subject to a D_3 CF potential.

Table 1. Transformation matrices to express the C_q^k operators in C_2 symmetry from D_3 symmetry.

$$\begin{bmatrix} C_0^2 \\ C_2^2 \end{bmatrix} = \begin{bmatrix} -\frac{1}{2} & -\frac{\sqrt{3}}{\sqrt{2}} \\ \frac{\sqrt{3}}{2\sqrt{2}} & -\frac{1}{2} \end{bmatrix} \times \begin{bmatrix} C_0^2 \\ 0 \end{bmatrix}$$

$$\begin{bmatrix} C_0^4 \\ C_2^4 \\ C_4^4 \\ \mathrm{i}C_2^4 \\ \mathrm{i}C_4^4 \end{bmatrix} = \begin{bmatrix} \frac{3}{8} & 0 \\ -\frac{\sqrt{5}}{4\sqrt{2}} & 0 \\ \frac{\sqrt{35}}{8\sqrt{2}} & 0 \\ 0 & -\frac{\sqrt{14}}{4} \\ 0 & -\frac{\sqrt{2}}{4} \end{bmatrix} \times \begin{bmatrix} C_0^4 \\ C_3^4 \end{bmatrix}$$

$$\begin{bmatrix} C_0^6 \\ C_2^6 \\ C_4^6 \\ C_6^6 \\ \mathrm{i}C_2^6 \\ \mathrm{i}C_4^6 \\ \mathrm{i}C_6^6 \end{bmatrix} = \begin{bmatrix} -\frac{5}{16} & 0 & -\frac{\sqrt{231}}{16} \\ \frac{\sqrt{105}}{32} & 0 & -\frac{3\sqrt{220}}{64} \\ -\frac{3\sqrt{7}}{16\sqrt{2}} & 0 & -\frac{\sqrt{66}}{32} \\ \frac{\sqrt{231}}{32} & 0 & -\frac{1}{32} \\ 0 & \frac{9}{16} & 0 \\ 0 & -\frac{\sqrt{30}}{8} & 0 \\ 0 & -\frac{\sqrt{55}}{16} & 0 \end{bmatrix} \times \begin{bmatrix} C_0^6 \\ C_3^6 \\ C_6^6 \end{bmatrix}$$

In the search for a reliable minimum in the fitting procedure, rough values of the six D_3 CF parameters to be used as starting parameters can be derived from two approaches. In the first, among the various theoretical models of the CF interactions [21] we have applied the *simple overlap model* SOM [22], a simplified *semi-empirical* calculation to obtain the initial CF set from the crystallographic structure. The consideration of the phenomenological set of CF parameters reported for Eu^{3+} in YAB [11] is another possibility. Free-ion parameters do not vary much for a given lanthanide ion in different systems, and consequently those initially used can be taken from the literature [23]. Their values were firstly refined up to giving the best barycenters of the energy levels as compared to experiment. This method is relatively simple,

and given the reduced number of CF parameters involved, constitutes a reliable simulation procedure. The following step supposes the transformation of the obtained CF parameters according to the indicated rotation making the c-axis of the CF collinear with the C_2 axis of the structure. In fact, for a refinement involving now so many CF parameters, the simulation is first operated in the C_{2v} symmetry, with only nine real B_q^k parameters, and when they are adequately fixed, the five complex S_q^k ones are added, carrying the calculation up to an unique consistent final set with all refined free-ion and CF parameters.

The correct procedure for the simulation of the energy level scheme of Nd^{3+} supposes the *simultaneous* treatment of both free-ion and CF effects using the *untruncated basis set* of wavefunctions. This scheme was used in present calculations, in contrast to previous ones carried out either for Nd^{3+} doped hexagonal YAB host [14, 15] or Nd^{3+} in hexagonal NAB [24]. In the first mentioned case, the phenomenological model [15] considered separately free-ion wavefunctions obtained by diagonalizing a Hamiltonian containing only the Coulomb and spin-orbit interactions, and after that the CF parameters were derived from the diagonalization of matrices representing CF interactions, in the strongly reduced basis of the $^4I_{9/2}$, $^4I_{11/2}$, $^4I_{13/2}$ and $^4F_{3/2}$ states. Barycenters of J-multiplets were assumed to be invariant even under the CF interaction, neglecting the effect of J-mixing. For Nd^{3+} in hexagonal NAB [24], B_q^k parameters were calculated through their quasi-three-parameter-method using as experimental data the Stark levels of $^4I_{9/2}$, $^4I_{11/2}$ and $^4F_{3/2}$ measured at 77 K.

Our best-fit sets of parameters correspond to the minimum of the rms function σ (see the bottom of table 5 for definition) obtained by least squares refinement between observed and calculated energy levels [25].

4. Results and discussion

Figure 2 shows as an example of our measurements the 7 K optical absorption of $^4F_{5/2}$, $^2H_{9/2}$ and $^4F_{9/2}$ Nd^{3+} multiplets in NAB. It is worth noting the strong polarization character of the spectra. It is also important to remark the presence of band pairs separated by 49 cm^{-1}. For each pair, the low energy band corresponds to a transition starting at the first excited level of the $^4I_{9/2}$ multiplet, therefore all these bands have been ignored for our purposes. When the local D_3 point site symmetry of Nd^{3+} in NAB is considered the CF interaction removes the $J + 1/2$ degeneracy of the $^{2S+1}L_J$ states of Nd^{3+}. These Stark levels are characterized by crystal quantum numbers $\mu = \pm 1/2$, $3/2^+$ or $3/2^-$ corresponding to $E_{1/2}$ or $A_{3/2}$, $A^*_{3/2}$ Kramers conjugate irreducible representations IR. Table 2 includes the number of these levels along with the corresponding IR for each J value.

Table 2. Irreducible representations of observed levels for the D_3 symmetry of Nd^{3+}.

J	Irreducible representation
1/2	$E_{1/2}$
3/2	$E_{1/2} + (A_{3/2},A^*_{3/2})$
5/2	$2E_{1/2} + (A_{3/2},A^*_{3/2})$
7/2	$3E_{1/2} + (A_{3/2},A^*_{3/2})$
9/2	$3E_{1/2} + 2(A_{3/2},A^*_{3/2})$
11/2	$4E_{1/2} + 2(A_{3/2},A^*_{3/2})$
13/2	$5E_{1/2} + 2(A_{3/2},A^*_{3/2})$
15/2	$5E_{1/2} + 3(A_{3/2},A^*_{3/2})$
17/2	$6E_{1/2} + 3(A_{3/2},A^*_{3/2})$

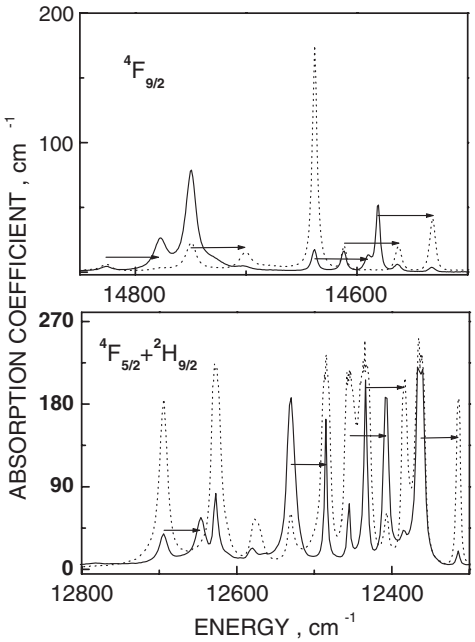

Figure 2. 7 K optical absorption of selected Nd^{3+} multiplets for NAB crystal. Continuous lines, π-spectrum. Dashed lines, s-spectrum. The arrows indicate bands of thermal origin separated by 49 cm^{-1}.

Table 3. Selection rules for induced electric dipole ED and magnetic dipole MD transitions for the D_3 symmetry of Nd^{3+}.

	ED		MD	
	$E_{1/2}$	$A_{3/2}, A^*_{3/2}$	$E_{1/2}$	$A_{3/2}, A^*_{3/2}$
$E_{1/2}$	α, σ, π	α, σ	α, σ, π	α, π
$A_{3/2}, A^*_{3/2}$	α, σ	π	α, π	σ

Table 3 summarizes the group theoretical selection rules of electric dipolar (ED) or magnetic dipolar (MD) transitions. α ($E \perp c$; $B \perp c$) and σ ($E \perp c$; $B \parallel c$) experimental spectra have been found equivalent, therefore the Nd^{3+} transitions observed are mainly ED. The crystal quantum number μ of $^2P_{1/2}$ is $1/2$, see table 2, and since it is observed in both σ and π spectra, the ground level from which this transition originates has also $\mu = 1/2$. Thus transitions from the ground Stark level to $\mu = 1/2$ levels will be observed simultaneously in σ and π spectra for both ED or MD transitions, and those to $\mu = 3/2^+, 3/2^-$ levels either in σ or π polarizations, for ED and MD mechanisms, respectively. The 135 experimental levels collected in table 4 have been labelled with the σ or π polarization character of the absorption or emission transitions and with the corresponding irreducible representation as discussed above.

According to the above values of μ, the observed energy levels of Nd^{3+} in NAB have been classified into two submatrices, the first one corresponding to $\mu = 1/2$ and the second one including $\mu = 3/2^+, 3/2^-$ levels. Each matrix is diagonalized separately in the fitting method. The second matrix will give wavefunctions transforming as one of two possible IRs associated with μ values distinguished by superscripts.

Table 4. 7 K observed (E_o) and calculated (E_c) energy levels (cm^{-1}) of Nd^{3+} in monoclinic $NdAl_3(BO_3)_4$. The energies of the levels were calculated with the parameter D_3-set b of table 5 and reduced $U^4/4$ tables. $^{*2S+1}L_J$ strongly mixed levels. The IR are in italic when they do not agree with the experimental observation.

$^{2S+1}L_J$	‖	IR	E_o	E_c	$^{2S+1}L_J$	‖	IR	E_o	E_c	$^{2S+1}L_J$	‖	IR	E_o	E_c
$^4I_{9/2}$	$\sigma\pi$	$E_{1/2}$	0	−7	$^4G_{5/2}$	$\sigma\pi$	$E_{1/2}$	16 862	16 867	$^4D_{5/2}$	$\sigma\pi$	$E_{1/2}$	28 035	28 015
	σ	$A_{3/2}, A^*_{3/2}$	49	56		$\sigma\pi$	$E_{1/2}$	17 034	17 050		$\sigma\pi$	$E_{1/2}$	28 249	28 255
	$\sigma\pi$	$E_{1/2}$	147	154		σ	$A_{3/2}, A^*_{3/2}$	17 063	17 070	$^4E_{1/2}$	$\sigma\pi$	$E_{1/2}$	28 411	28 400
	σ	$A_{3/2}, A^*_{3/2}$	271	298	$^4G_{7/2}$	$\sigma\pi$	$E_{1/2}$	17 170	17 185	$^2I_{11/2}$	$\sigma\pi$	$E_{1/2}$	28 812	28 833
	$\sigma\pi$	$E_{1/2}$	323	348	$^2G_{7/2}$	$\sigma\pi$	$E_{1/2}$	17 249	17 231		σ	$A_{3/2}, A^*_{3/2}$	29 008	29 032
$^4I_{11/2}$	$\sigma\pi$	$E_{1/2}$	1934	1928	$^2G_{7/2}$	$\sigma\pi$	$E_{1/2}$	17 282	17 263		$\sigma\pi$	$E_{1/2}$	29 036	29 049
	σ	$A_{3/2}, A^*_{3/2}$	1948	1940	$^2G_{7/2}$	σ	$A_{3/2}, A^*_{3/2}$	17 338	17 342			$A_{3/2}, A^*_{3/2}$	—	29 286
	$\sigma\pi$	$E_{1/2}$	1964	1962	$^4G_{7/2}$	$\sigma\pi$	$E_{1/2}$	18 809	18 791		$\sigma\pi$	$E_{1/2}$	29 317	29 315
	$\sigma\pi$	$E_{1/2}$	2083	2086	$^4G_{7/2}$	$\sigma\pi$	$E_{1/2}$	18 873	18 872			$E_{1/2}$	—	29 345
	σ	$A_{3/2}, A^*_{3/2}$	2104	2103	$^2G_{7/2}$	$\sigma\pi$	$A_{3/2}, A^*_{3/2}$	18 925	18 932	$^2L_{15/2}$	$\sigma\pi$	$E_{1/2}$	29 787	29 767
	$\sigma\pi$	$E_{1/2}$	2142	2143	$^4G_{7/2}$	$\sigma\pi$	$E_{1/2}$	18 990	18 990	$^2L_{15/2}$		$A_{3/2}, A^*_{3/2}$	—	29 846
$^4I_{13/2}$	π	$A_{3/2}, A^*_{3/2}$	3898	3891	$^2K_{13/2}$	σ	$A_{3/2}, A^*_{3/2}$	19 249	19 255	$^2L_{15/2}$	$\sigma\pi$	$E_{1/2}$	29 848	29 860
	$\sigma\pi$	$E_{1/2}$	3908	3881	$^2K_{13/2}$	$\sigma\pi$	$E_{1/2}$	19 283	19 288	$^4D_{7/2}$		$E_{1/2}$	—	29 896
	$\sigma\pi$	$E_{1/2}$	3924	3910	$^4G_{9/2}$	$\sigma\pi$	$A_{3/2}, A^*_{3/2}$	19 369	19 369	$^2L_{15/2}$	σ	$A_{3/2}, A^*_{3/2}$	29 991	30 025
	$\sigma\pi$	$E_{1/2}$	4044	4037	$^4G_{9/2}$	$\sigma\pi$	$E_{1/2}$	19 375	19 375	$^2L_{15/2}$		$E_{1/2}$	—	30 098
	$\sigma\pi$	$E_{1/2}$	4075	4064	$^4G_{9/2}$	$\sigma\pi$	$E_{1/2}$	19 394	19 414	$^4D_{7/2}$	$\sigma\pi$	$E_{1/2}$	30 119	30 133
	σ	$A_{3/2}, A^*_{3/2}$	4097	4091	$^4G_{9/2}$	$\sigma\pi$	$E_{1/2}$	19 425	19 423	$^2L_{15/2}$	$\sigma\pi$	$E_{1/2}$	—	30 162
	$\sigma\pi$	$E_{1/2}$	4147	4139	$^4G_{9/2}$	σ	$A_{3/2}, A^*_{3/2}$	19 451	19 437	$^4D_{7/2}$		$A_{3/2}, A^*_{3/2}$	—	30 203
$^4I_{15/2}$	$\sigma\pi$	$E_{1/2}$	5851	5847	$^2K_{13/2}$		$E_{1/2}$	—	19 494	$^4D_{7/2}$	$\sigma\pi$	$E_{1/2}$	30 209	30 222
	σ	$A_{3/2}, A^*_{3/2}$	5857	5840		$\sigma\pi$	$E_{1/2}$	19 569	19 575	$^2L_{15/2}$		$A_{3/2}, A^*_{3/2}$	—	30 241
	$\sigma\pi$	$E_{1/2}$	5924	5940		$\sigma\pi$	$E_{1/2}$	19 699	19 682	$^{*2}I_{13/2}(^2L_{15/2})$	$\sigma\pi$	$E_{1/2}$	30 269	30 281
	$\sigma\pi$	$E_{1/2}$	6073	6092		σ	$A_{3/2}, A^*_{3/2}$	19 788	19 778	$^2I_{13/2}$	$\sigma\pi$	$E_{1/2}$	30 304	30 306
	σ	$A_{3/2}, A^*_{3/2}$	6099	6105		$\sigma\pi$	$E_{1/2}$	19 820	19 817	$^2I_{13/2}$	$\sigma\pi$	$E_{1/2}$	30 389	30 384
		$E_{1/2}$	—	6173	$^2G1_{9/2}$	$\sigma\pi$	$E_{1/2}$	20 807	20 778	$^2I_{13/2}$	σ	$A_{3/2}, A^*_{3/2}$	30 498	30 500
	σ	$A_{3/2}, A^*_{3/2}$	6220	6224		σ	$A_{3/2}, A^*_{3/2}$	20 829	20 806	$^2I_{13/2}$	$\sigma\pi$	$E_{1/2}$	30 517	30 501
	$\sigma\pi$	$E_{1/2}$	6281	6286		$\sigma\pi$	$E_{1/2}$	20 905	20 925	$^2I_{13/2}$	σ	$A_{3/2}, A^*_{3/2}$	30 654	30 655

Table 4. (Continued)

$^{2S+1}L_J$	‖	IR	E_o	E_c	$^{2S+1}L_J$	‖	IR	E_o	E_c	$^{2S+1}L_J$	‖	IR	E_o	E_c
$^4F_{3/2}$	$\sigma\pi$	$E_{1/2}$	11 364	11 353		σ	$A_{3/2}, A^*_{3/2}$	20 920	20 904	$^2I_{13/2}$		$E_{1/2}$	—	30 676
	σ	$A_{3/2}, A^*_{3/2}$	11 436	11 418		σ	$E_{1/2}$	21 003	21 012	$^2I_{13/2}$	$\sigma\pi$	$E_{1/2}$	30 699	30 702
$^4F_{5/2}$	$\sigma\pi$	$E_{1/2}$	12 363	12 341	$^2D_{3/2}$	$\sigma\pi$	$E_{1/2}$	21 075	21 092	$^2L_{17/2}$		$E_{1/2}$	—	31 294
	$\sigma\pi$	$E_{1/2}$	12 432	12 426		σ	$A_{3/2}, A^*_{3/2}$	21 122	21 140	$^2L_{17/2}$	σ	$A_{3/2}, A^*_{3/2}$	31 302	31 298
	σ	$A_{3/2}, A^*_{3/2}$	12 455	12 467	$^4G_{11/2}$	$\sigma\pi$	$E_{1/2}$	21 171	21 186	$^2L_{17/2}$	$\sigma\pi$	$E_{1/2}$	31 376	31 380
$^2H2_{9/2}$	$\sigma\pi$	$E_{1/2}$	12 530	12 546	$^4G_{11/2}$	σ	$E_{1/2}$	21 213	21 227	$^2L_{17/2}$	$\sigma\pi$	$E_{1/2}$	31 523	31 522
	σ	$E_{1/2}$	12 576	12 572	$^4G_{11/2}$	σ	$A_{3/2}, A^*_{3/2}$	21 306	21 317	$^2L_{17/2}$	σ	$A_{3/2}, A^*_{3/2}$	31 606	31 592
	$\sigma\pi$	$A_{3/2}, A^*_{3/2}$	12 627	12 626	$^2K_{15/2}$	$\sigma\pi$	$E_{1/2}$	21 365	21 353	$^2L_{17/2}$		$E_{1/2}$	—	31 628
	$\sigma\pi$	$E_{1/2}$	12 694	12 690	$^2K_{15/2}$	$\sigma\pi$	$E_{1/2}$	21 383	21 360	$^2L_{17/2}$		$E_{1/2}$	—	31 675
		$A_{3/2}, A^*_{3/2}$	—	12 717	$^2K_{15/2}$	σ	$A_{3/2}, A^*_{3/2}$	21 443	21 439	$^2L_{17/2}$		$A_{3/2}, A^*_{3/2}$	—	31 730
$^4F_{7/2}$	$\sigma\pi$	$E_{1/2}$	13 337	13 351	$^4G_{11/2}$	$\sigma\pi$	$E_{1/2}$	21 498	21 499	$^2L_{17/2}$	$\sigma\pi$	$E_{1/2}$	31 756	31 758
	$\sigma\pi$	$A_{3/2}, A^*_{3/2}$	13 364	13 370	$^2K_{15/2}$	σ	$A_{3/2}, A^*_{3/2}$	21 533	21 529	$^2H_{9/2}$	—	$A_{3/2}, A^*_{3/2}$	32 556	32 579
	σ	$E_{1/2}$	13 417	13 419	$^2K_{15/2}$		$E_{1/2}$	—	21 577		—	$E_{1/2}$	32 609	32 590
$^4S_{3/2}$	$\sigma\pi$	$E_{1/2}$	13 472	13 464	$^4G_{11/2}$	$\sigma\pi$	$E_{1/2}$	21 621	21 620		—	$E_{1/2}$	32 651	32 657
$^4S_{3/2}$	—	$A_{3/2}, A^*_{3/2}$	—	13 470	$^4G_{11/2}$	σ	$A_{3/2}, A^*_{3/2}$	21 675	21 673			$A_{3/2}, A^*_{3/2}$	—	32 684
$^4F_{7/2}$	$\sigma\pi$	$E_{1/2}$	13 483	13 494	$^2K_{15/2}$		$E_{1/2}$	—	21 718		—	$E_{1/2}$	32 695	32 696
$^4F_{9/2}$	π	$E_{1/2}$	14 580	14 575	$^2K_{15/2}$	σ	$A_{3/2}, A^*_{3/2}$	21 796	21 772	$^2D2_{3/2}$	—	$A_{3/2}, A^*_{3/2}$	33 050	33 054
	$\sigma\pi$	$E_{1/2}$	14 611	14 607	$^2K_{15/2}$	$\sigma\pi$	$E_{1/2}$	21 813	21 804		—	$E_{1/2}$	33 095	33 094
	σ	$A_{3/2}, A^*_{3/2}$	14 638	14 635	$^2P_{1/2}$	$\sigma\pi$	$E_{1/2}$	23 131	23 130	$^2D2_{5/2}$	—	$A_{3/2}, A^*_{3/2}$	33 885	33 911
	$\sigma\pi$	$E_{1/2}$	14 749	14 760	$^2D_{5/2}$	$\sigma\pi$	$E_{1/2}$	23 628	23 624	$^2D2_{5/2}$	—	$E_{1/2}$	33 934	33 931
	$\sigma\pi$	$A_{3/2}, A^*_{3/2}$	14 826	14 835		σ	$A_{3/2}, A^*_{3/2}$	23 697	23 712	$^2H1_{11/2}$		$E_{1/2}$	-	33 946
$^2H2_{11/2}$	$\sigma\pi$	$E_{1/2}$	15 790	15 816		$\sigma\pi$	$E_{1/2}$	23 786	23 789	$^2H1_{11/2}$	—	$A_{3/2}, A^*_{3/2}$	33 988	34 005
	$\sigma\pi$	$E_{1/2}$	15 816	15 845	$^2P_{3/2}$	$\sigma\pi$	$E_{1/2}$	26 006	25 984	$^2H1_{11/2}$	—	$E_{1/2}$	34 041	34 030
	σ	$A_{3/2}, A^*_{3/2}$	15 827	15 840		σ	$A_{3/2}, A^*_{3/2}$	26 094	26 072	$^2H1_{11/2}$		$E_{1/2}$	—	34 064
	σ	$A_{3/2}, A^*_{3/2}$	15 936	15 949	$4D_{3/2}$	$\sigma\pi$	$E_{1/2}$	27773	27773	$^2H1_{11/2}$		$A_{3/2}, A^*_{3/2}$	—	34 092
	$\sigma\pi$	$E_{1/2}$	15 974	15 964		σ	$A_{3/2}, A^*_{3/2}$	27 805	27 780	$^2D2_{5/2}$	—	$E_{1/2}$	34 175	34 154
	$\sigma\pi$	$E_{1/2}$	16 000	15 996	$^4D_{5/2}$		$A_{3/2}, A^*_{3/2}$	—	27 969	$^2H1_{11/2}$	—	$E_{1/2}$	34 215	34 171

The large number of observed energy levels, 135, table 4, together with the rational number of CF parameters imposed by the symmetry, assure certainly a reasonable determination of both the atomic and CF parameters. The possible exception is γ, whose value is partially determined by available data although is strongly dependent on the position of the missing ^{2}F levels. Since the splitting of the $^2H2_{11/2}$ state is not adequately reproduced by the classical one-electron CF model [21, 26] the corresponding six observed energy levels have not been used in this CF parametrization. The simulation was carried out with a very satisfactory rms deviation, $\sigma = 15.1$ cm^{-1}, table 5 (D_3, set a). Even more important, no large discrepancies between the calculated and experimental values of individual energy levels are observed, with the exception of the two last observed levels ($^2H1_{11/2}$ and $^2D2_{5/2}$), that present strong J-mixing. In fact, the inclusion of higher excited levels with increasing J-mixing slightly changes the best fit B_q^k set and impairs somewhat the overall simulation. Table 5 (D_3, set a) summarizes the collection of parameters for the best fit. Its good quality is also verified by the low standard deviation values of the parameters.

For the crystallographic C_2 symmetry of monoclinic NAB in the Nd^{3+} site the $J + 1/2$ degeneracy of the $^{2S+1}L_J$ states of Nd^{3+} is also completely removed to Kramers levels. These Stark levels are characterized by crystal quantum numbers $\mu = 1/2^+$ or $1/2^-$, corresponding to $A_{1/2}$, $A_{1/2}^*$ Kramers conjugate IR. But in this case all ED and MD transitions between levels are allowed, and optical spectra should not present particular characteristics depending on the polarization of the beam light. Thus, the fitting procedure cannot distinguish these levels, and *one unique matrix* with all of them is diagonalized. Since the constraints imposed by group theory in the parametrization of CF effects are now nonexistent, it is not straightforward to fit the data with a total Hamiltonian. The number of adjustable parameters is very large, and in this case nonlinear least squares fits are unreliable, resulting in several minima that can be indistinguishable from the point of view of the quality of the fit. Given that the optimized parameter set is very dependent on the chosen starting values, imposing theoretical constraints can alleviate these difficulties. In this case, taking into account that the total CF strength for the C_2 site must be strictly the same than the previously evaluated for D_3 symmetry, the initial set of transformed from D_3 to C_2 parameters has been the obvious choice, table 5 ($D_3 \rightarrow C_2$). The simulation converged rapidly to the best CF parameters given in table 5 (C_2, set a), with a very low σ value, 14.1 cm^{-1}. These CF parameters are, in fact, very close to those initially predicted from the phenomenological fit for D_3.

As indicated above, the current adjustments provide the usual bad reproduction of the splitting of the $^2H2_{11/2}$ multiplet [26], including the modification of the distribution of these energy levels in both submatrices for D_3, that is their sequence of crystal quantum numbers. This phenomenon is known to be more pronounced as the fourth order CF parameters are stronger with respect to the second and sixth order parameters [27, 28]. For Nd^{3+} in NAB the experimental $^2H2_{11/2}$ splitting amounts to 210 cm^{-1}, and the calculated ones are 51 and 56 cm^{-1}, for D_3 and C_2 respectively. The difference is even more flagrant than for the classical example Nd_2O_3, 280 and 97 cm^{-1}, respectively. The non-negligible mixing with levels of the excited $4f^25d^1$ configuration could be included in CF fits to account for these poorly fitted levels, through the odd CF parameters and/or charge transfer and spin and orbitally correlated CF models [29, 30]. Thus, the introduction of two-electron CF interactions has been considered. The difficulty lies in the large number of parameters that are required to represent the various two-electron operators that can be added to the CF Hamiltonian without violating any symmetry constraints. It is argued [31] that the most elementary way to introduce these two-electron interactions is to replace each component $(C_q^k)_i$ of the single electron tensor $C^{(k)}$ for electron i occurring in the conventional CF Hamiltonian for $c_k(\boldsymbol{S}\cdot\boldsymbol{s})(C_q^k)_i$. The c_k ($k = 2$, 4, 6) experimentally adjustable parameters must necessarily be negative if the contraction of

Table 5. Free ion and CF parameters (cm^{-1}) for Nd^{3+} in monoclinic $NaAl_3(BO_3)_4$ crystal. Italics indicate CF parameters calculated from SOM ($\rho = 0.06$; effective charge for oxygen $= -0.8$). Sets a do not include $^2H2_{11/2}$ levels, and sets b stand for results using reduced $U^4/4$ tables. Values in parentheses refer to estimate standard deviations in the indicated parameter.

		D_3				C_2	
	SOM	Set a	Set b		$D_3 \rightarrow C_2$	Set a	Set b
E^0		23 487.7 (9)	23 488.3 (9)	E^0		23 492.5 (9)	23 485.5 (9)
E^1		4841.4 (7)	4850.4 (7)	E^1		4846.3 (6)	4845.0 (7)
E^2		23.23 (1)	23.24 (1)	E^2		23.25 (1)	23.25 (1)
E^3		480.72 (7)	480.94 (7)	E^3		479.8 (7)	480.03 (7)
α		21.08 (3)	21.17 (2)	α		20.99 (2)	21.15 (2)
β		−629 (3)	−631 (3)	β		−626 (3)	−631 (3)
γ		1233 (4)	1186 (4)	γ		[1200]	[1200]
ζ		868.6 (6)	866.6 (6)	ζ		869.7 (6)	868.8 (6)
$M^{0,a}$		0.58 (6)	0.40 (6)	$M^{0,a}$		0.79 (6)	0.60 (6)
$P^{2,b}$		196 (13)	191 (13)	$P^{2,b}$		224 (13)	191 (13)
T^2		321 (2)	315 (2)	T^2		351 (2)	347 (2)
T^3		40 (2)	39 (2)	T^3		41 (2)	41 (2)
T^4		80 (2)	84 (2)	T^4		75 (2)	81 (2)
T^6		−274 (4)	−273 (4)	T^6		−269 (4)	−270 (4)
T^7		316 (5)	323 (5)	T^7		316 (5)	328 (5)
T^8		271 (6)	276 (5)	T^8		285 (5)	297 (5)
B_0^2	*183*	452 (9)	450 (9)	B_0^2	*−225*	−205 (13)	−215 (13)
B_0^4	*−1783*	−1516 (23)	−1516 (23)	B_2^2	*276*	296 (6)	292 (16)
B_3^4	*−868*	−945 (19)	−940 (19)	B_0^4	*−569*	−604 (50)	−591 (53)
B_0^6	*997*	514 (27)	537 (27)	B_2^4	*599*	559 (28)	596 (27)
B_3^6	*−370*	−245 (24)	−254 (24)	S_2^4	*879*	793 (21)	791 (21)
B_6^6	*−431*	−427 (24)	−412 (24)	B_4^4	*−792*	−674 (24)	−661 (25)
				S_4^4	*332*	673 (27)	670 (26)
				B_0^6	*224*	208 (51)	186 (51)
				B_2^6	*458*	375 (25)	387 (26)
				S_2^6	*−143*	7 (36)	−22 (37)
				B_4^6	*−84*	−24 (46)	−43 (50)
				S_4^6	*174*	195 (29)	175 (29)
				B_6^6	*268*	363 (26)	365 (27)
				S_6^6	*118*	235 (40)	229 (41)
S_2	*82*	202	201	S_2	*201*	209	208
S_4	*722*	674	672	S_4	*672*	672	673
S_6	*355*	240	241	S_6	*241*	245	244
S_T[c]	*467*	429	428	S_T[c]	*428*	430	430
l		129	135	l		129	135
σ^d		15.1	15.3	σ^d		14.1	14.7
Residue		24 275.1	26 292.3	Residue		19 930.9	22 958.3

[a] M^0, M^2, M^4 were constrained by the ratios $M^2 = 0.5625\ M^0$, $M^4 = 0.3125\ M^0$.
[b] P^2, P^4, P^6 were constrained by the ratios $P^4 = 0.50\ P^2$, $P^6 = 0.10\ P^2$.
[c] $S_k = \left\{1/(2k+1)\left[(B_0^k)^2 + 2\sum_q[(B_q^k)^2 + (S_q^k)^2]\right]\right\}^{1/2}$ $\qquad S_T = \left[\frac{1}{3}\sum_k S_k^2\right]^{1/2}$.
[d] $\sigma = \left[\sum(\Delta_i)^2/(l-p)\right]^{1/2}$, l number of Stark levels, p number of parameters.

the radial functions is to correspond to similarly directed spins. In this way the number of supplementary spin correlated CF parameters is low. Keeping in mind that the simulation of the whole energy level scheme of Nd^{3+} in NAB is the target, the action of the c_k parameters on the splitting of the $^2H2_{11/2}$ multiplet was examined for both D_3 and C_2 considered CF potentials.

They were maintained around the limits $|c_2| \leqslant 0.05$, $|c_4| \leqslant 0.1$ and $|c_6| \leqslant 0.3$, and when fixed to these negative values we observed that their combined action even worsened the reproduction of the splitting of this multiplet, which drops to about 30 cm^{-1}. Obviously, total final σ are also deteriorated.

Putting aside the idea of finding the physical reason of the phenomenon, some empirical manipulations have proved to be successful in reproducing the correct sequence [26]. Among them, the division of the $\langle {}^2H2_{11/2}|U^4|{}^2H2_{11/2}$ reduced matrix element by 4 improves the simulation of the $^2H2_{11/2}$ splitting for Nd^{3+} in NAB almost without changing the CF parameter values, and reduces the residues as well as the rms standard deviations. Results of the above parametrizations, including all 135 observed energy levels, are given in table 5 (D_3-set b and C_2-set b). Figure 3(a) shows the results for our three carried out simulations, with 129 energy levels, $U^4/4$ reduced tables and Judd's parameters, in each case, for the $^2H2_{11/2}$ multiplet in D_3 symmetry. Figure 3(b) shows a similar plot for other selected multiplets. Table 4 contains the D_3 calculated energy level sequence of Nd^{3+} in NAB, for which $^2H2_{11/2}$ energy levels are included, and in any case the calculated C_2 energy sequence is very similar.

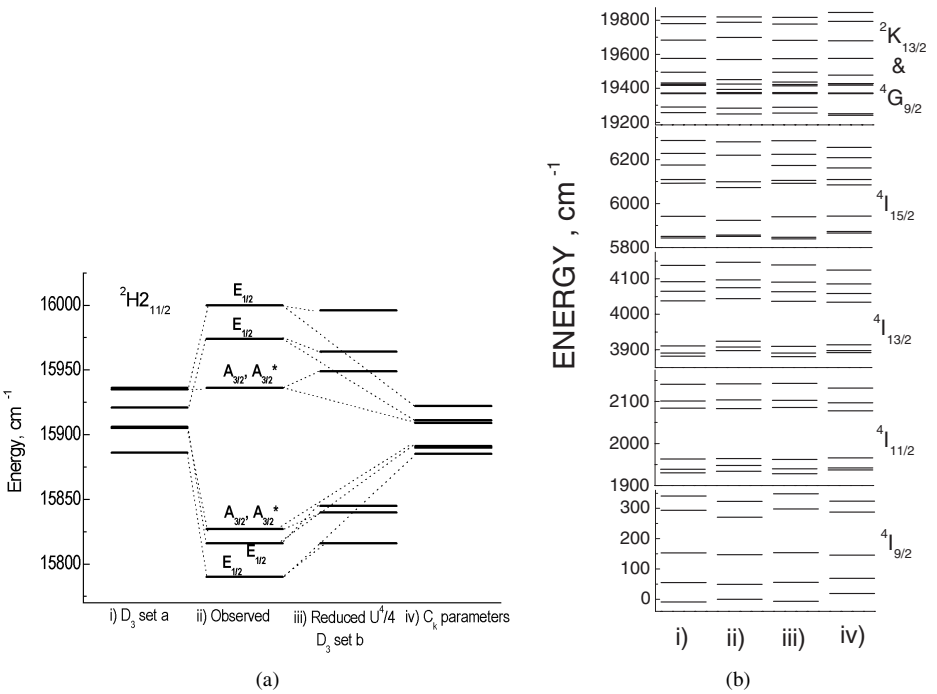

Figure 3. Diagram of the splitting of the observed and calculated multiplet of Nd^{3+} in NAB: (i) calculated with parameters D_3, set a, table 5; (ii) experimentally observed levels; (iii) calculated with D_3, set b; (iv) including c_k parameters. (a) Detail of the $^2H2_{11/2}$ multiplet. (b) General overview of selected multiplets.

The careful analysis of table 5 reveals some noteworthy results: (i) for the same CF potential considered, neither free-ion nor CF parameters substantially vary when $^2H2_{11/2}$ energy levels and $U^4/4$ reduced tables are used, (ii) phenomenological CF strengths, S_k, from D_3 and C_2 CF potentials present values extremely close independently of the k rank, (iii) although the inclusion of more CF parameters in C_2 with respect to D_3 obviously drops

the σ and residue values, the standard deviations estimated for each C_2 CF parameter are higher, especially for B_0^4 and B_0^6. While the first point indicates the validity of the empirical correction for the calculated $^2H2_{11/2}$ anomalous splitting, the last one supports the D_3 local symmetry of Nd^{3+} in monoclinic NAB assumed according to the polarization rules experimentally found. The confidence and physical meaning of these fits are indicated by the low s values obtained. Moreover, these results allow us to consider the sequence of observed levels as unambiguously assigned. The labelling of levels has been made according to the main component of the wavefunction, and due to the complexity of the composition of each wavefunction one given label can appear more than expected, table 4. For instance, around 30 000 cm^{-1}, only seven energy positions having a $^2L_{15/2}$ main component instead of eight are listed. On the other hand, eight Stark components are contributing to the main wavefunction component of $^2I_{13/2}$ instead of seven. Hence, we conclude that the levels on the higher-energy side are more disturbed by mixing along with other effects than at the lower side. This is an indication of the strong mixing of wavefunctions associated with these levels.

Table 5 also contains the starting CF parameters obtained from SOM. There is a general similarity between CF strengths S_k for semi-empirical and calculated sets of data. Regarding previous CF results for Eu^{3+} in hexagonal YAB [11, 22], and as must be expected, the value of B_0^2 describing the long-range CF interaction, as well as B_0^4, and B_0^6 are very similar for both configurations. The higher B_3^6 and B_6^6 values observed for Eu^{3+} seem to be related, among other facts, to the reduced number of ^7F_J levels, 21, used in the Eu^{3+} CF parametrization. Phenomenological CF sets for Nd^{3+} are anyway closer to SOM values than those of Eu^{3+}.

On the other hand, there are significant differences, in values and also in signs, between results of this work and those from previous CF analyses of Nd^{3+} in hexagonal NAB [24] and Nd^{3+} doped hexagonal YAB host [14, 15], as well as, more surprisingly, between these last ones. For Nd^{3+} in hexagonal NAB and YAB matrices the reason for the disparity was attributed to differences in the sequence of experimentally determined energy levels used (13 and 20 levels, respectively) and their assigned IR in each case. Initially, the minimum obtained for NAB through the proposed quasi-three-parameter method was claimed to be the only solution corresponding to the physical reality [24]; however, the second fit was afterward considered more confidently by reason of its lower rms value. Accurately determined extended schemes of energy levels is the first condition for a consistent CF analysis, and in these conditions when the same lanthanide cation is embedded in an isostructural host, either as a constituent or as an impurity, only a few variations can be expected in final fit CF parameters. In this way, although initially different CF effects for Nd^{3+} in monoclinic NAB could be anticipated, from the above explained considerations on the local symmetry around Nd^{3+} it is easy to predict that the total CF strengths will be almost the same as those of the hexagonal NAB crystal. In the simulations on Nd^{3+} in the hexagonal host, the J-mixing effect does not play obviously any significant role in low-lying Stark levels, particularly ^4I multiplets that are well separated from other multiplets; that is, the truncature has only a very small influence on these lower energy levels, but the deviation enlarges towards the truncation edge [32]. Anyway, the effect of J-mixing and the interaction with excited configurations, which cannot be ignored in the phenomenological calculation of the sequence of levels of the configuration, along with detailed free-ion interactions, must be accounted through the consideration of well determined high-lying multiplets.

Finally, the experimental results presented so far and the above CF calculations support the hypothesis of a unique Nd^{3+} site in NAB. On the other hand, high-resolution excitation spectra of the $^4F_{3/2} \rightarrow {}^4I_{9/2}$ transition suggest that the observed optical absorption bands could be the convolution of two Nd^{3+} centers [33]. The nature of the environment of these two possible

Nd^{3+} centers is not obvious. The possibility of Nd^{3+} replacing Al^{3+} in NAB (two different Al^{3+} in monoclinic NAB versus one single position in the hexagonal phase) have been evaluated by semi-empirical SOM estimations of the CF parameters from their atomic coordinates, although the details are not given for the sake of brevity. This model only considers the first coordination sphere around Nd^{3+}, that is Nd–O distances now equal to the Al–O distances in NAB. The CF strengths calculated are considerably higher than can be reasonably thought. Therefore, this assumption can be clearly discarded. It seems likely to us that the origin of the two centers could be related to distortions of the local Nd environment in NAB or even to some degree of mixing between C_2 and D_3 site symmetries.

5. Conclusions

The comparison between experimental results provided by polarized optical spectroscopy, OA and PL measurements at 7 K and the energies provided by the crystal field theory allows a meaningful assignment of the experimental Nd^{3+} energy levels in monoclinic $NdAl_3(BO_3)_4$ single crystal. Despite the crystal belonging to the $C2/c$ space group symmetry, a local D_3 symmetry of the Nd^{3+} site is able to reproduce very well the experimental energy level sequence. The hypothetical contribution to the spectra of Nd^{3+} ions in Al sites can be clearly ignored.

Acknowledgment

Work supported by Comisión Interministerial Cienca y Technología under projects MAT99-1077, PB97-1200 and PB97-0033.

References

[1] Winzer G, Möckel P G and Krühler W W 1978 *IEEE J. Quantum Electron.* **14** 840
[2] Zundu Luo, Ai-dong Jiang, Yi-chuan Huang and Min-Wang Qiu 1991 *Sci. China* A **34** 762
[3] Jaque D, Enguita O, García Solé J, Jiang A D and Luo Z D 2000 *Appl. Phys. Lett.* **76** 2176
[4] Wang G, He M and Luo Z 1991 *Mater. Res. Bull.* **26** 108
[5] Hong H Y P and Dwight K 1974 *Mater. Res. Bull.* **9** 1661
[6] Belokoneva E L, Simonov M A, Pashkova A V, Timchenko T I and Belov N V 1980 *Sov. Phys.–Dokl.* **25** 948
[7] Jarchow P, Lutz F and Klaska K H 1979 *Z. Kristallogr.* **149** 162
[8] Luzt F and Huber G 1981 *J. Cryst. Growth* **52** 646
[9] Leask M J M, Maxwell K J and Wanklyn B 1967 *J. Chem. Phys.* **47** 3665
[10] Kellendonk F and Blasse G 1981 *J. Chem. Phys.* **75** 561
[11] Görller-Walrand C, Vandevelde P, Hendrickx I, Porcher P, Krupa J C and King G S D 1988 *Inorg. Chim. Acta* **143** 259
[12] Jaque D, Capmany J, Luo Z D and García Solé J 1997 *J. Phys.: Condens. Matter* **9** 9715
[13] Zundu Luo and Yidong Huang 1993 *J. Phys.: Condens. Matter* **5** 6949
[14] Yidong Huang and Zundu Luo 1991 *Phys. Status Solidi* **167** K117
[15] Xeyuan Chen and Zundu Luo 1998 *J. Phys.: Condens. Matter* **10** 5147
[16] Prather J L 1961 *Atomic Energy Levels in Crystals (US National Bureau of Standards Monograph)*
[17] Wybourne G 1965 *Spectroscopic Properties of Rare Earths* (New York: Wiley–Interscience)
[18] Caro P, Derouet J, Beaury L, Teste de Sagey G, Chaminade J P, Aride J and Pouchard M 1981 *J. Chem. Phys.* **74** 2698
[19] Porcher P, Svoronos D R, Leskelä M and Hölsä J 1983 *J. Solid State Chem.* **46** 101
[20] Beaury L, Derouet J, Escorne M and Porcher P 1994 *J. Phys.: Condens. Matter* **6** 5169
[21] Garcia D and Faucher M 1995 Crystal field in non-metallic (rare earth) compounds *Handbook on the Physics and Chemistry of Rare Earths* vol 21, eds K A Gschneidner Jr and L Eyring (Amsterdam: North-Holland) p 263 (and references therein)
[22] Porcher P, Couto dos Santos M and Malta O 1999 *Phys. Chem. Chem. Phys.* **1** 397

[23] Carnall W T, Goodman G L, Rajnak K and Rana R S 1989 *J. Chem. Phys.* **90** 3443
[24] Yidong Huang and Zundu Luo 1993 *J. Phys.: Condens. Matter* **5** 1581
[25] Porcher P 1999 Fortran routines REEL and IMAGE for simulation of d^N and f^N configurations involving real and complex crystal field parameters, unpublished.
[26] Faucher M, Garcia D, Antic-Fidancev E and Lemaitre Blaise M 1989 *J. Phys. Chem. Solids* **50** 1227
[27] Faucher M, Garcia D, Derouet J and Caro P 1989 *J. Physique* **50** 219
[28] Faucher M, Garcia D and Porcher P 1989 *C. R. Acad. Sci. Paris* **II 308** 603
[29] Newman D J, Siu G G and Fung W Y P 1982 *J. Phys. C: Solid State Phys.* **15** 3113
[30] Judd B R 1977 *Phys. Rev. Lett.* **34** 242
[31] Judd B R J 1989 *J. Phys. C: Solid State Phys.* **13** 2695
[32] Teste de Sagey G, Porcher P, Garon G and Caro P 1982 *The Rare Earths in Modern Science and Technology* vol 3, ed G J McCarthy, H B Silber and J J Rhyne (New York: Plenum) p 127
[33] Jaque D, Enguita O, Caldiño U, Ramírez M O, García Solé J, Zaldo C, Muñoz-Santiuste J E, Gian J and Luo Z D *J. Appl. Phys.* **90** 561